Atomic Site-Sensitive Processes in Low Energy Ion-Dimer Collisions

W. Iskandar,[1] J. Matsumoto,[2] A. Leredde,[3] X. Fléchard,[4,*] B. Gervais,[1] S. Guillous,[1] D. Hennecart,[1] A. Méry,[1] J. Rangama,[1] C. L. Zhou,[1] H. Shiromaru,[2] and A. Cassimi[1]

[1]*CIMAP, CEA-CNRS-ENSICAEN, BP 5133, F-14070 Caen Cedex 5, France*

[2]*Department of Chemistry, Tokyo Metropolitan University, 1-1 Minamiosawa, Hachiouji-shi, Tokyo 192-0397, Japan*

[3]*Physics Division, Argonne National Laboratory, Argonne, Illinois 60439, USA*

[4]*LPC Caen, ENSICAEN, Université de Caen, CNRS/IN2P3, 14050 Caen Cedex 04, France*

(Received 2 May 2014; revised manuscript received 31 July 2014; published 2 October 2014)

Electron capture processes for low energy Ar^{9+} ions colliding with Ar_2 dimer targets are investigated, focusing attention on charge sharing between the two Ar atoms as a function of the molecular orientation and the impact parameter. A preference for charge-asymmetric dissociation channels is observed, with a strong correlation between the projectile scattering angle and the molecular ion orientation. The measurements here provide clear evidence that projectiles distinguish each atom in the target and that electron capture from near-site atoms is favored. Monte Carlo calculations based on the classical over-the-barrier model, with dimer targets represented as two independent atoms, are compared to the data. They give new insight into the dynamics of the collision by providing, for the different electron capture channels, the two-dimensional probability maps $p(\vec{b})$, where $\vec{b}$ is the impact parameter vector in the molecular frame.

DOI: 10.1103/PhysRevLett.113.143201 PACS numbers: 34.70.+e, 34.10.+x, 36.40.Mr

Investigating an elementary reaction with a well-defined geometry, where the orientation of the reactant is fixed in space and the impact parameter is well controlled, is a challenging subject that has the potential to considerably deepen the understanding of chemical reactions. Using molecular orientation techniques [1,2] or event-by-event measurements to determine *a posteriori* the molecular orientation at the instant of the collision [3,4], the orientation dependence in collisions involving highly charged ions (HCIs) has now been studied over a broad energy range [3–9]. For fast collisions (with projectile velocities v_p higher than the active electron velocities v_e) leading to multiple ionization of the target, the orientation dependence was first qualitatively understood by a geometrical model [5,10] and later interpreted using the statistical energy deposition model [4,6]. In the specific case of dimer targets, the molecular orientation dependence helped in the identification of one-step (one-site) versus two-step (two-site) processes [8], or allowed for the determination of the impact-parameter-dependent ionization probability $p(b)$ for atomic scattering processes [9]. Determination of the impact parameter vector $\vec{b}$ in the molecular frame is a more delicate issue. Since Rutherford's gold foil scattering experiment, access to the impact parameter is provided by the exchange of transverse momentum between the projectile and the target. In the case of molecular targets, a measurement of the molecular orientation and of the transverse momentum exchange are both required.

A charged projectile generates a highly localized electric field, and it is then natural to expect preferential ionization or capture from near-site atoms to occur. Access to such atomic site sensitivity of the processes relies on the observation of the induced asymmetry in the final charge sharing between the molecular fragments as a function of the impact parameter vector $\vec{b}$ in the molecular frame. For fast collisions inducing very small transverse momentum exchange and with a significant contribution of the emitted electrons, such a measurement seems out of reach. But for multiple electron capture processes resulting from low energy ($v_p \ll v_e$) HCI-molecule collisions, the transverse momentum exchanged between the projectile and the center of mass of the molecule may become measurable. One difficulty remains: namely that the observed asymmetry is the result of the final charge sharing on the molecular fragments, and the latter can be significantly altered by intramolecular charge redistribution. If the electron mobility between the two atomic sites is high, Coulomb repulsion between the ionized molecular target and the projectile ion would lead to a lower charge on the near site. Such behavior has been observed for N_2 covalent molecules in very low energy collisions (less than 100 eV/u) [7]. In contrast, if the electron mobility in the molecule is low, the near site should remain preferentially ionized. In a previous paper, we have shown that asymmetric charge sharing is favored in the fragmentation of argon dimers multiply ionized by electron capture in low energy collisions with Ar^{9+} projectiles [11]. The preference of asymmetric to symmetric sharing in the dimer case was interpreted in terms of the low electron mobility. We present here an experimental and theoretical study of atomic site sensitivity for this collision system, providing new insight into the multiple-electron capture processes for ion-molecule collisions.

The full details of the apparatus and data analyses are described in Refs. [11,12]. The beam of 15 qkeV Ar^{9+} ions was generated with an electron cyclotron resonance ion source at the ARIBE-GANIL facility (Caen, France) and the Ar_2 dimer target was provided by a supersonic gas jet. Recoil ions resulting from charge transfer were collected using a uniform electric field and detected using a microchannel plate position sensitive detector (MCPPSD). A −3 kV post-acceleration voltage was applied on the front plate of the MCPPSD to ensure maximal detection efficiency for all ion charge states [13]. Fragment ions from the dimers were identified by time of flight (TOF) coincidence measurements triggered by the detection of scattered projectiles on a second MCPPSD. To determine the kinetic energy release (KER) of the fragmentation and the orientation of the dissociating dimer, the momentum of each fragment ion in the center of mass was calculated from the position and TOF data, imposing a momentum conservation restriction for optimal resolution and background suppression [14]. The novelty, here, is that the transverse momentum transferred to the dimer center of mass during the collision was also inferred from these data sets, giving direct access to the transverse components of the momentum of the scattered projectile [15]. In spite of a resolution limited by the finite size of the collision region, the scattering angle of the projectile and its angle of emission, ϕ_{proj}, were determined with sufficient precision for the present study.

As the setup was only sensitive to charged fragments, processes resulting in the emission of a neutral Ar atom were not detected. The fragmentation channels that were observed, (i) $Ar_2^{2+} \rightarrow Ar^+ + Ar^+$ for double capture (DC), (ii) $Ar_2^{3+} \rightarrow Ar^{2+} + Ar^+$ for triple capture (TC), and (iii) $Ar_2^{4+} \rightarrow Ar^{3+} + Ar^+$ and $Ar_2^{4+} \rightarrow Ar^{2+} + Ar^{2+}$ for quadruple capture (QC), are, respectively, denoted by $(1,1)_F$, $(2,1)_F$, $(3,1)_F$, and $(2,2)_F$. Their relative detected yields (without selection on the molecular orientation) and contributions from the different capture processes are shown in Fig. 1. The relative uncertainties are purely statistical and remain below 3%. For quadruple capture, Fig. 1 clearly shows the preference for the asymmetric fragmentation channel resulting from the low electron mobility between the two atoms of the dimer. Each fragmentation channel can be fed by different initial capture processes corresponding to a given number of electrons removed from each site during the collision, prior to any possible charge redistribution. The $(1,1)_F$ fragmentation channel can result from "two-site" double capture $(1,1)_C$ leading directly to Coulomb explosion, but also from "one-site" double capture $(2,0)_C$ populating nondissociative molecular states (using the same notation for capture and fragmentation channels, with respectively the subscripts C and F). As previously shown [11,12], these transient states relax through radiative charge transfer (RCT) towards the same dissociative states as $(1,1)_C$, but at shorter internuclear distances. While ending up in the same fragmentation channel $(1,1)_F$, the two processes can still be distinguished by their different KER. An estimate of their contributions is given in Fig. 1. The KER distributions of the two processes partly overlap [11] and about 20% of the events could not be clearly attributed to the $(2,0)_C$ or to the $(1,1)_C$ channel. Transient nondissociative molecular states populated by one-site TC and QC, denoted $(3,0)_C$ and $(4,0)_C$, lead to the $(2,1)_F$ and $(3,1)_F$ fragmentation channels, respectively, through direct crossing with excited states. They can thus not be experimentally isolated from the $(2,1)_C$ and $(3,1)_C$ capture channels.

In the present study, we focus on the angular correlation between the scattered projectile and the recoiling fragments for the different electron capture scenarios. To obtain a clearer view of the impact parameter dependence in the molecular frame, we limit here the analysis to molecular targets oriented perpendicular to the beam axis at the

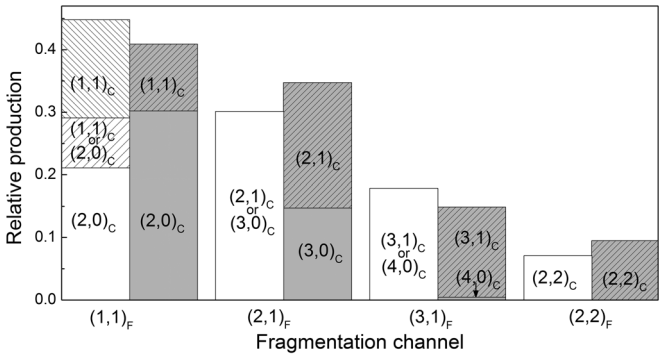

FIG. 1. Relative yields for the different electron capture and fragmentation channels extracted from the experimental data (white) and results from MC-COBM calculations (gray).

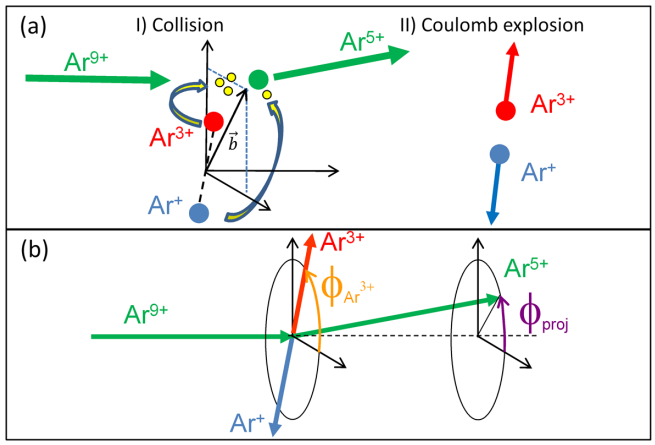

FIG. 2 (color online). Schematic view of the multiple electron capture from Ar_2 by Ar^{9+} projectiles resulting in the $(3,1)_F$ asymmetric fragmentation channel (a). Representation of the scattering angle ϕ_{proj} and of the angle of emission $\phi_{Ar^{3+}}$ of the most charged fragment in the plane transverse to the beam axis (b).

moment of the collision. As schematically illustrated in Figs. 2(a) and 2(b), the projectile scattering angle ϕ_{proj} is given by the direction of the transverse momentum exchange arising from the Coulomb repulsion between the collision partners. It is thus closely related to the impact parameter vector $\vec{b}$ in the molecular frame and to the final charge on the two sites of the molecule. In Fig. 2(b), the molecular orientation is defined by the angle $\phi_{\mathrm{Ar}^{3+}}$. In the general case, it is defined by the angle of the most charged fragment, $\phi_{\mathrm{Ar}^{A+}}$, and serves as a reference to determine the projectile scattering angle in the molecular frame, $\phi_{\mathrm{diff}} = \phi_{\mathrm{proj}} - \phi_{\mathrm{Ar}^{A+}}$.

The angular distributions in ϕ_{diff} are shown in Fig. 3 for a selection of the data corresponding to dimer target orientations close to 90° (60°–120°). They were symmetrized about the horizontal axis to account for the symmetry of the collision system. For symmetric fragmentation channels, the two fragments are no longer distinguishable and the ϕ_{diff} reconstruction accounts for an additional symmetry about the vertical axis. The distributions of the $(1,1)_C$ and $(2,2)_C$ symmetric channels reach their maximum at 90° and 270°, indicating dominant impact parameters close to the median plane of the dimer internuclear axis. For the

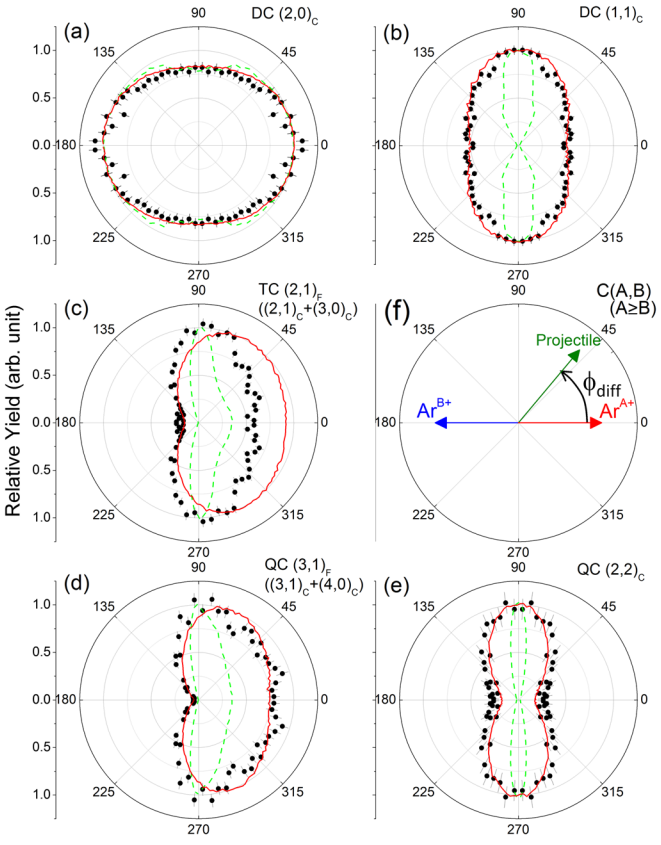

FIG. 3 (color online). Angular distributions in ϕ_{diff} for the DC (a),(b), TC (c), and QC (d),(e) electron capture and associated fragmentation channels. Experimental data (black dots) are compared to the calculations with (red lines) and without (dashed green lines) convolution with the experimental function response.

channels $(2,1)_F$ and $(3,1)_F$, a strong asymmetry is observed, with projectiles preferentially scattered in the direction of the most charged fragment. In the simple picture of the collision given by Fig. 2, it is clearly evident that electron capture from the near site is favored. For the channel $(2,0)_C$, we end up with a symmetric distribution: one cannot distinguish experimentally which fragment was initially ionized, prior to the RCT decay process that finally leads to the $(1,1)_F$ symmetric charge sharing. This loss of memory of the initial capture process leads to a quasi-isotropic angular distribution. An angular asymmetry for the initial $(2,0)_C$ capture process could thus only be clearly evidenced using appropriate calculations.

For low energy ion-atom collisions leading to multiple capture, the classical over-the-barrier model (COBM) [16] is known to be quite reliable. An analytical treatment of the $\mathrm{Ar}^9 + \mathrm{Ar}_2$ collision based on this model and considering the dimer target as two Ar atoms fixed in space has already been performed [17]. However, the calculations relied on an adjustable screening coefficient and they did not give access to the projectile scattering angle. We use here a similar method that combines the improved version of the COBM described by Niehaus [18] with Monte Carlo (MC) simulations. The orientation of the molecule with respect to the beam axis as well as the impact parameter vector $\vec{b}$ in the molecular frame are randomly determined. For the two argon atoms, the radii of "capture spheres" corresponding to the target-projectile distances at which target electrons become "molecular," when the Coulomb barrier decreases on the incoming path ("way in"), and at which they can be captured, when the Coulomb barrier increases on the outgoing path ("way out"), are computed according to Ref. [18]. The crossing points between the projectile trajectory and the capture spheres of the two argon atoms are then determined sequentially in the straight-line trajectory approximation for each simulated event. For crossing points of the way out, capture by the projectile or recapture by the atomic target of "molecular electrons" is determined randomly using probability weights proportional to the respective phase space available on the projectile and on the target [18]. If the two Ar atoms are here considered as fully independent, one site can still influence the interaction between its neighbor and the projectile. On the way out of the collision, this interaction can be affected by the possible change of the projectile charge induced by electron capture from the other site. The sequential treatment allowed by a MC simulation is thus an essential feature of the model: along the projectile trajectory, one can follow all the crossing points with capture spheres and the subsequent charge sharing between the three partners of the collision. The MC simulation approach also enables the transverse momentum exchange due to Coulomb repulsion to be computed, and thus to determine the projectile scattering angle. For this, we simply consider that the charge of the molecular electrons shared by the

projectile and the Ar atoms on the way in is distributed between the different partners, while in the way out, the charge of captured electrons is transferred from the target to the projectile. Finally, the event-by-event mode of the MC-COBM approach gives access to the correlation between the initial conditions (impact parameter vector $\vec{b}$ and molecule orientation) and the outcome of the collision (capture multiplicity on each site and the projectile scattering angle).

The relative yields obtained with this method for the different capture configurations are compared to the experimental results in Fig. 1. As for the experimental data, calculations were first performed taking into account all the molecular orientations. For "one-site" TC $(3,0)_C$ and QC $(4,0)_C$, 50% of the populations given by the calculations can be statistically attributed to transient nondissociative molecular states. They are thus added to the final $(2,1)_F$ and $(3,1)_F$ fragmentation channels, respectively, fed through direct crossings by these nondissociative states. Similarly, we also account for the 50% of the DC $(2,0)_C$ population that dissociates prior to RCT and does not end up in the $(1,1)_F$ fragmentation channel. Without any adjustable parameter included in the model, the results are found to be in very good agreement with the data. To be compared with the more detailed experimental results of Fig. 3, the angular distributions in ϕ_{diff} obtained with the MC COBM have been convoluted with the instrumental resolution, given by the 0.6 mm (FWHM) diameter of the collision region. As for the data, we have selected dimer target orientations between 60° and 120°. After including these instrumental effects, calculations are once again found to be in excellent agreement with the experiment for most of the capture or fragmentation channels. A substantial discrepancy can only be seen for the $(2,1)_F$ channel, where the angular asymmetry predicted by the model is stronger than in the experimental data. This could be simply explained by an overestimation of the $(3,0)_C$ capture channel in the calculations. To further test the model, the mean value of the transverse momentum exchange, $\langle P_\perp \rangle$, was also extracted and compared to the experiment for each process. A good overall agreement was obtained, with a systematic underestimation of $P_\perp$ by about 25% due to the simplistic charge repartition chosen for the way in of the collision. These classical calculations do not account for most of the complex interactions and mechanisms at play in the multiple capture process. Nevertheless, the good agreement with the data, in particular for the ϕ_{diff} distributions, demonstrates that the model gives a realistic picture of the multiple capture process for structured targets such as rare gas dimers.

Now, the MC COBM provides direct access to the impact parameter $p(\vec{b})$ in the molecular frame. The 2D maps in $p(\vec{b})$ leading to the different capture scenarios are displayed in Fig. 4 for dimer targets oriented at 90°. The color scale indicates the number of events for the simulation for each capture channel of interest at a given impact parameter $\vec{b}$. The circular steplike structures correspond to the intersections of projectile trajectories with the different capture spheres involved in the process. More complex structures also arise from the fact that electron capture from one site changes the projectile charge state, and thus the probability to capture other molecular electrons from the second site. Vertical structures visible at intersection planes between two capture spheres arise in such a manner: in the way out, projectile trajectories located on one side of a plane cross first the capture sphere of the site from the other side. For asymmetric capture configurations, and in particular for $(2,0)_C$, we clearly confirm that capture from the near site is strongly favored. Impact parameters that contribute most to these processes cover a large area on the side of the most charged fragment. For the symmetric capture channels, contributing impact parameters are restrained close to the median plane of the internuclear axis, which partly explains the predominance of asymmetric over symmetric fragmentation channels.

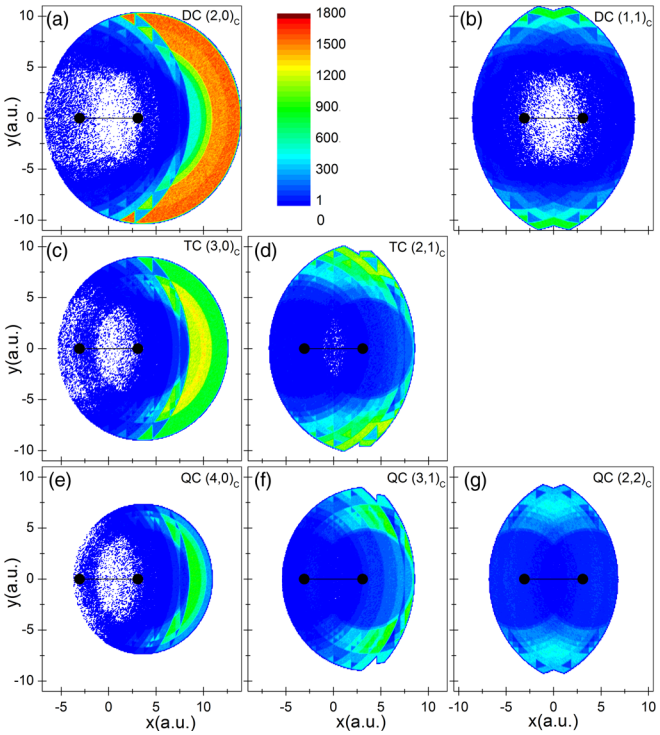

FIG. 4 (color online). 2D maps $p(\vec{b})$ in the molecular frame for the different capture processes ($\vec{b}$ is in atomic units). The color scale indicates the number of events resulting from the MC-COBM simulation, the areas in white corresponding to no event. Positions of the atomic sites are indicated by black dots with the higher final charge state on the right.

To summarize, measurements of the angular correlation between the scattered projectile and the recoiling fragments combined with model calculations have provided access to atomic site sensitivity in low energy collisions between HCIs and Ar_2 dimers. It is seen that electron capture from

"near-site" atoms is strongly favored, as opposed to what was previously observed with N_2 covalent molecules [7], and may be a specific feature of rare gas dimer targets owing to the low electron mobility. The same methodology could be employed to investigate the atomic site dependence for different projectile charges and for more complex targets, such as larger homonuclear or mixed clusters.

We thank the CIMAP and GANIL staff for their contribution in the preparation of the experiment. This work is partly supported by TMU Research Program in the financial years 2013–2014.

*flechard@lpccaen.in2p3.fr

[1] K. H. Kramer and R. B. Bernstein, J. Chem. Phys. **42**, 767 (1965).
[2] H. Sakai, S. Minemoto, H. Nanjo, H. Tanji, and T. Suzuki, Phys. Rev. Lett. **90**, 083001 (2003).
[3] V. Horvat, O. Heber, R. L. Watson, R. Parameswaran, and J. M. Blackadar, Nucl. Instrum. Methods Phys. Res., Sect. B **99**, 94 (1995).
[4] U. Werner, N. M. Kabachnik, V. N. Kondratyev, and H. O. Lutz, Phys. Rev. Lett. **79**, 1662 (1997).
[5] C. Caraby, A. Cassimi, L. Adoui, and J. P. Grandin, Phys. Rev. A **55**, 2450 (1997).
[6] B. Siegmann, U. Werner, Z. Kaliman, Z. Roller-Lutz, N. M. Kabachnik, and H. O. Lutz, Phys. Rev. A **66**, 052701 (2002).
[7] M. Ehrich, U. Werner, H. O. Lutz, T. Kaneyasu, K. Ishii, K. Okuno, and U. Saalmann, Phys. Rev. A **65**, 030702(R) (2002).
[8] J. Titze *et al.*, Phys. Rev. Lett. **106**, 033201 (2011).
[9] H.-K. Kim *et al.*, Phys. Rev. A **89**, 022704 (2014).
[10] K. Wohrer and R. L. Watson, Phys. Rev. A **48**, 4784 (1993).
[11] J. Matsumoto *et al.*, Phys. Rev. Lett. **105**, 263202 (2010).
[12] J. Matsumoto *et al.*, Phys. Scr. **T144**, 014016 (2011).
[13] C. Couratin *et al.*, Phys. Rev. A **88**, 041403(R) (2013).
[14] Th. Weber *et al.*, J. Phys. B **34**, 3669 (2001).
[15] A. Cassimi, S. Duponchel, X. Flechard, P. Jardin, P. Sortais, D. Hennecart, and R. Olson, Phys. Rev. Lett. **76**, 3679 (1996).
[16] A. Bárány, G. Astner, H. Cederquist, H. Danared, S. Huldt, P. Hvelplund, A. Johnson, H. Knudsen, L. Liljeby, and K.-G. Rensfelt, Nucl. Instrum. Methods Phys. Res., Sect. B **9**, 397 (1985).
[17] T. Ohyama-Yamaguchi and A. Ichimura, Phys. Scr. **T144**, 014028 (2011).
[18] A. Niehaus, J. Phys. B **19**, 2925 (1986).